Implications of Passive Mixer Transparency for Impedance Matching and Noise Figure in Passive Mixer-First Receivers

Caroline Andrews, *Student Member, IEEE*, and Alyosha C. Molnar, *Member, IEEE*

***Abstract*—In this paper, a class of passive mixer-first, LNA-less receivers is analyzed in depth. Quadrature passive mixers are shown to present the impedance of their baseband port to the RF port and *vice versa*. This transparency property, in combination with resistive feedback differential amplifiers, and "complex" feedback between the I and Q paths, can be used to control the impedance at the RF port. This impedance can be tuned using only baseband components (i.e., resistors). The noise limits of such an architecture are analyzed and simulated, and are shown to be comparable to standard RF-LNA-first receivers. Accounting for the higher harmonics of the LO frequency proves critical in accurately analyzing the behavior of these circuits and their ability to provide an impedance match with low noise figure. Additionally, it is shown that expanding quadrature passive mixers to harmonic rejection mixers allows for even better noise performance and wider matching range.**

***Index Terms*—Impedance matching, noise figure, passive mixer-first receiver, RF CMOS receiver.**

I. Introduction

DEMAND for highly integrated, multifunction wireless transceivers has exploded over the last decade, driving innovations in radio architecture to permit on-the-fly programmability of various radio parameters. Although many key parameters have been made fully flexible, the physical interface to the antenna has not. Recently, a receiver architecture was presented where the antenna directly interfaces to a passive mixer and provides highly flexible baseband controlled impedance matching without significant degradation of performance (especially noise figure and linearity) [1]. In this paper we present the theoretical background for such baseband programmable RF impedance matching and bandpass filtering through a passive mixer as well as analyze the noise performance of this class of receiver.

After the matching network, traditional receivers have an LNA that must be low noise, provide power gain, and exhibit good linearity, while providing an input impedance that is matched. This is not entirely straightforward: a simple resistive matching network always results in a noise figure above 3 dB. In fact, a reasonable definition for an LNA is an amplifier which provides a real impedance match while maintaining a sub-3 dB noise figure. For applications requiring low noise figure and a good impedance match, a resonant antenna impedance matching network is typically used. Such a network's passive RF components are not easily tunable over a wide range of values [2], [3]. To make matters worse, the impedance of the antenna and matching network is strongly frequency dependent, severely limiting channel tuning range for high performance receivers.

Because performance tradeoffs tend to fall so heavily on the receiver front end, and involve relatively inflexible components, many multiband systems that receive a range of frequencies use multiple, parallel front-ends, tuned to different frequencies, using distinct matching networks and LNAs [4], [5]. Alternatively, an LNA with wideband impedance matching and good noise figure *can* be achieved using either a wideband amplifier with resistive feedback [6], [7], or with a noise-canceled LNA [8]. Such designs intrinsically require large amounts of power to operate at RF frequencies while maintaining a constant antenna impedance, and still generally provide a relatively fixed input impedance. At the other extreme, applications requiring low power consumption and cost can simply forgo the matching network and LNA completely, connecting directly to a passive mixer [9], [10].

As gate lengths continue to fall, smaller, faster MOSFETs allow sampling passive mixers to operate in the gigahertz range with better linearity and lower power consumption than traditional active mixers [9]–[11]. These circuits have unusual properties, such as very high linearity [10] and a capacity to pass the impedance presented at one port (i.e., the baseband port) to the other port (i.e., the RF port) [12]. This transparency property has been used to translate baseband filtering onto a mixer's RF port, suppressing wideband interference [1], [9], [13], [14]. So far, these improvements have come at the cost of significantly higher noise figure (typically 5–6 dB) [1], [9], [10].

In this paper, we analyze the transparency of passive mixers in detail, especially analyzing a method by which this transparency can be used to provide a baseband-tunable, complex impedance match to the antenna. The bidirectional nature of passive mixers also causes their noise figure to depend strongly on the circuits at both the RF and IF interfaces [12]. Here we analyze the fundamental dependencies between RF and IF impedance and limits on both matching and noise figure (NF). We show that both NF and matching can be made competitive with traditional LNA-first receivers, while providing high-Q front end filtering (which is good for linearity: [1], [10]) and extreme frequency

Manuscript received December 01, 2009; revised March 31, 2010; accepted May 02, 2010. Date of publication July 23, 2010; date of current version December 15, 2010. This paper was recommended by Associate Editor E. A. M. Klumperink.

The authors are with Cornell University, Ithaca, NY 14853 USA (e-mail: cja67@cornell.edu).

Digital Object Identifier 10.1109/TCSI.2010.2052513

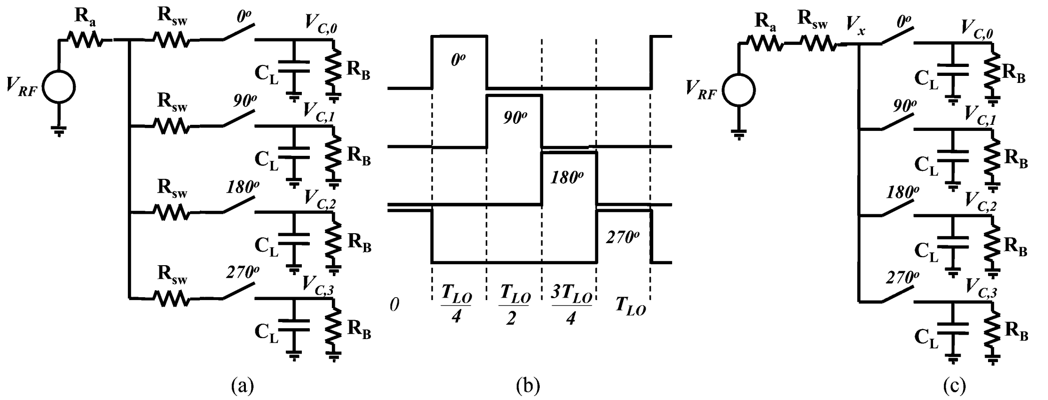

Fig. 1. (a) Simplified circuit model of 4-phase passive mixer. (b) LO driving waveforms. (c) Equivalent model to (a), with R_{sw} lumped with R_a based on nonoverlapping nature of the waveforms in the middle.

tuning range. These advantages imply that passive mixer-first receivers will likely provide the next step in improving the flexibility and performance of highly integrated wireless receivers.

II. Passive Mixer Transparency: First-Order Analysis

The passive mixer analyzed here contains four switches (transistors) which are successively turned on in four nonoverlapping, 25% duty-cycle phases over the course of one local oscillator (LO) period [1], [10], [15]–[17]. These nonoverlapping pulses are necessary for preventing the I-Q crosstalk described in [12]. The input port of the mixer is connected directly to the antenna port. The switches sample the RF voltage onto four capacitors loaded by the baseband resistors R_B. The phase-split nature of the LO, the mixer, and hence the amplifiers produces differential baseband signals with both I (from the 0° and 180° switches) and Q (from 90° and 270°) components.

A. Impedance Analysis

The analysis begins with a simplified model of a 4-phase passive mixer with nonoverlapping, 25% duty cycle, quadrature LO pulses, as shown in Figs. 1(a) and 1(b). The model treats the switches as ideal except for a small series resistance, R_{sw}, which represents the on-resistance of the switching MOSFET. Since the LO pulses are completely nonoverlapping, only one R_{sw} is active at a time, so the series resistance of all of the switches can be lumped together and treated as a single resistor of the same value, as shown in Fig. 1(c).

If we treat the antenna impedance as a resistor R_a (neglecting its reactive components for the moment), then the entire RF portion of the circuit can be modeled as a single lumped series combination of R_a and R_{sw} in series with a parallel array of four ideal switches. We can define an effective antenna resistance

$$R_a' = R_{sw} + R_a. \tag{1}$$

We now define a virtual voltage V_x at the node in bewteen R_{sw} and the ideal switches. The baseband port of the switches is loaded by the parallel combination of a filtering capacitor C_L and the amplifier input resistance, R_B. If the time constants R_BC_L and $R_a'C_L$ are significantly larger than the LO period, T_{LO}, then we can approximate these capacitors as holding their voltage constant over a given LO cycle. For in-band signals, the input from the antenna can be approximated as a sinusoid with fundamental frequency $\omega_{LO} = 2\pi/T_{LO}$ and time varying phase $\phi(t)$ and amplitude $A(t)$, which capture both modulation and offset frequency of the received signal. If the amplitude and phase offset change slowly relative to T_{LO} they can be approximated as constant over a given LO period, and the input can be approximated as

$$V_{RF}(t) = A\cos(\omega_{LO}t + \phi). \tag{2}$$

To compute the input impedance presented by the mixer to the antenna, we start by computing the voltage across each of the output capacitors in response to the input. Specifically, each capacitor will continuously dissipate current through its resistive load, R_B, such that the mth capacitor $(m = 0, 1, 2, 3)$ dissipates a current of $I_{C,m} = V_{C,m}/R_B$. For a full cycle of the LO, assuming $R_BC_L \gg T_{LO}$, this corresponds to a charge of $Q_m = T_{LO}V_{C,m}/R_B$. Meanwhile, for each cycle of the LO, this charge is replenished from the antenna during the quarter cycle during which the mth switch is closed. Assuming that the voltage across the mth capacitor, $V_{C,m}$ is at steady state (that is, assuming $\phi(t)$ and $A(t)$ change slowly relative to the time constants R_BC_L and $R_a'C_L$), conservation of charge implies that charge dissipated by R_B is balanced by the integral of the input current during a given quarter-LO cycle. To simplify this and future integrals, we also introduce a time shift in the integration limits of $-T_{LO}/8$

$$Q_m = \frac{V_{C,m}T_{LO}}{R_B} = \int_{mT_{LO}/4 - T_{LO}/8}^{(m+1)T_{LO}/4 - T_{LO}/8} \frac{V_{RF} - V_{C,m}}{R_a'}dt \quad m = 0, 1, 2, 3. \tag{3}$$

Substituting in (2) for V_{RF} and solving for $V_{C,m}$ results in the expression:

$$V_{C,m} = \frac{2\sqrt{2}}{\pi}\frac{R_B}{R_B + 4R_a'}A\cos\left(\phi + \frac{m\pi}{2}\right). \tag{4}$$

Note that this implies that that the output of the mixer depends not just on the strength of the RF input, but on the *relative* impedance of the antenna (R_a') compared to the baseband (R_B).

Passive mixers allow current to flow in both directions through the switches, from the RF port to the IF, and back. This means there will be a return or reradiation current generated by the difference between the voltage levels maintained on the filter

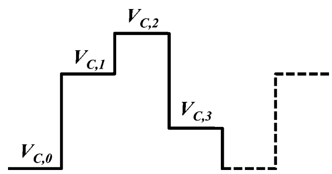

Fig. 2. Approximation of waveform V_x from Fig. 1.

capacitors of the mixer and the input on the antenna. Because the virtual voltage at V_x in Fig. 1(c) is always short-circuited to one of the output capacitors, it can be described by a stair-step waveform (shown in Fig. 2) with four phases corresponding to the four phases of the LO, and with a voltage at each phase corresponding to one of the output capacitors.

In order to characterize the effective impedance seen by the antenna, we find the current flowing out of the antenna into the receiver. In the time domain this will be

$$I_A(t) = \frac{V_{RF}(t) - V_x(t)}{R'_a}. \tag{5}$$

We will now look for the impedance seen by the antenna for a near-zero-IF system, where $\omega_{RF} \approx \omega_{LO}$. To find $I_A(t)$ we extract the component of V_x that resides at this frequency using a Fourier series representation of the signal over a period of time T_{LO}, and extract the fundamental term. Substituting (4) into the waveform (shown in Fig. 2) yields a term for the fundamental at ω_{LO}

$$\begin{aligned} V_{x,fund}(t) &= A\frac{8}{\pi^2}\frac{R_B}{R_B + 4R'_a}\cos(\omega_{LO}t + \phi) \\ &= V_{RF}(\omega_{LO})\frac{8}{\pi^2}\frac{R_B}{R_B + 4R'_a} \end{aligned} \tag{6}$$

from which we can compute $I_{A,fund}(t)$

$$\begin{aligned} I_{A,fund}(t) &= \frac{V_{RF}(t) - V_{x,fund}(t)}{R'_a} \\ &= V_{RF}(t)\frac{4R'_a + \left(\frac{1-8}{\pi^2}\right)R_B}{R'_a R_B + 4{R'_a}^2}. \end{aligned} \tag{7}$$

The current described in (7) looks like the input V_{RF} transformed by a combination of R'_a and R_B. Several observations can be made from (7). The first is that as $R_B \rightarrow 0$, $I_A \rightarrow V_{RF}/R'_a$, implying that R'_a acts in series with R_B. The second is that as $R_B \rightarrow \infty$, $I_A \rightarrow V_{RF}(1 - 8/\pi^2)/R'_a$, implying that there is additional antenna-dependent shunting in parallel with R_B. This leads us to introduce the time-invariant model in Fig. 3 for the original time-varying circuit in Fig. 1. This circuit accounts for the linear time-varying (LTV) effects of the switches with an impedance transform term γ acting on R_B, and an additional resistance R_{sh}, in shunt with the baseband resistance R_B. R_{sh} emerges from the charge balance in (3). However, as we will show in Section III-A, R_{sh} *in fact represents power lost due to upconversion by harmonics of the LO* through the switches to the antenna.

Given the model in Fig. 3 we can write a simple expression for its current I_A

$$I_A(\omega_{LO}) = V_{RF}(\omega_{LO})\frac{\gamma R_B + R_{sh}}{R'_a\gamma R_B + R'_a R_{sh} + R_{sh}\gamma R_B}. \tag{8}$$

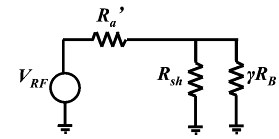

Fig. 3. LTI equivalent circuit for passive mixer with R_{sh} due to harmonics and impedance-transformed R_B.

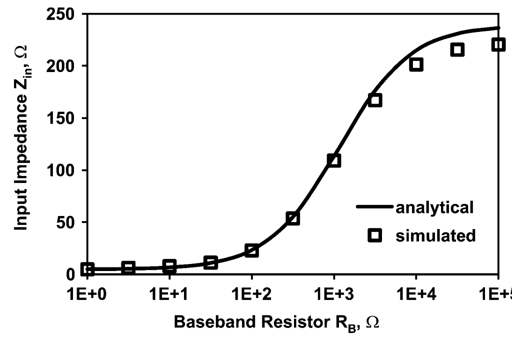

Fig. 4. Simulated and analytical equivalent input impedance R_{in} versus swept baseband resistor R_B.

To find the values for the scaling factor γ and the virtual shunt resistance R_{sh}, we set the current in our LTV circuit (7) equal to the current for our LTI model (8)

$$\gamma = \frac{2}{\pi^2} \approx 0.203 \tag{9}$$

$$R_{sh} = R'_a\frac{4\gamma}{1 - 4\gamma} \approx 4.3R'_a. \tag{10}$$

Note that while R_{sh} is proportional to R'_a in (10), this only holds as long as R_a is constant across all frequencies, once this ceases to be true, a more complex description is required, as explored in Section V.

B. Consequence: Impedance Matching

This model for the passive mixer shows that the impedance seen by the antenna through a quadrature passive mixer consists of the parallel combination of R_{sh} and γR_B in series with the switch resistance R_{sw}. Specifically, this impedance becomes

$$R_{in} = R_{sw} + \gamma R_B \| R_{sh}. \tag{11}$$

This result indicates that the impedance seen at the antenna interface can be modified by changing R_B. In particular, (11) shows that changing baseband resistance can be used to tune the input resistance R_{in} over a range that is limited by the properties of the mixer

$$R_{sw} < R_{in} < R_{sw} + R_{sh}. \tag{12}$$

We have confirmed this impedance analysis using numerical circuit simulation (PSS and PSP analyses in SpectreRF) of Fig. 1, with NMOS transistors as the switches. We choose transistor dimensions such that $R_{sw} = 5\ \Omega$, and choose $R_a = 50\Omega$, $C_L = 200$ pF, $f_{LO} = 100$ MHz, and $f_{RF} = f_{LO} + 1$ kHz. As can be seen in Fig. 4, sweeping R_B from 10 Ω to 100 kΩ and applying (11) analytically predicts numerical, periodic steady-state simulations with high accuracy. The resulting curve shows that for very high values of R_B, the effective R_{in} converges to near R_{sh}, and that for very low values of R_B, R_{in}

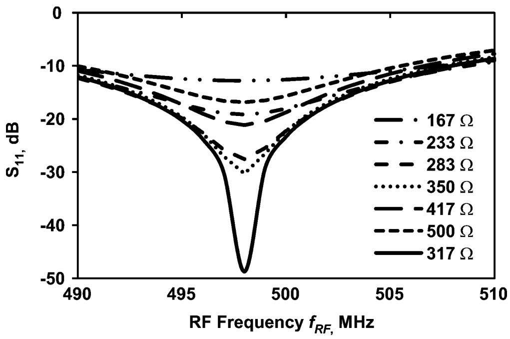

Fig. 5. Simulated S_{11} for varying R_B.

converges to R_{sw}. The difference in the two curves for large R_B values is due to the parasitic shunt capacitance present on the antenna side of the switch, which changes the effective R'_a (and therefore R_{sh}) as the RF frequency increases. The effects of a frequency-dependent R_a will be examined in Sections III and V.

The limits in (12) imply that an impedance match, where $R_{in} = R_a$, can be achieved provided that $R_{sw} < R_a$ and $R_{sh} > R_a - R_{sw}$. As we will show, maintaining switch resistance such that $R_{sw} \ll R_a$ is also desirable from a noise perspective, and can usually be achieved in a modern process. Equation (11) implies that when antenna impedance R_a is treated as constant and real, and $R_{sh} > R'_a$, an impedance match can always be achieved by choosing R_B such that

$$R_B = \frac{1}{\gamma}\frac{R_{sh}R_a - R_{sw}R_{sh}}{R_{sw} + R_{sh} - R_a}. \quad (13)$$

We have confirmed the impedance matching ability of the circuit in Fig. 1 with periodic S-parameter analysis for swept R_B. Here we have chosen $f_{LO} = 500$ MHz and $C_L = 50$ pF, with other circuit parameters the same as in Fig. 4. Fig. 5 shows that a real RF impedance match with $S_{11} < -45$ dB can be achieved through passive mixer directly connected to the antenna port.

There are two additional features to notice about Fig. 5. The first is that the match is fairly narrowband. We will show in Section III-B. that the shape of this match as a function of ω_{IF} is in fact determined by the capacitor C_L. The second is that the center frequency of the match is slightly shifted from the LO. We will show in Section V that this offset is due to complex antenna impedance, and demonstrate a method by which the location of this optimal match can be controlled.

III. Effects of Frequency-Dependent Components

A. Accounting for Harmonic Conversion

In the previous section, we defined the up-converted voltage V_x only at the fundamental of the LO, or ω_{LO}. However, its stairstep nature seen in Fig. 2 indicates that V_x contains odd harmonics of the LO as well as its fundamental. These harmonics in V_x come from the up-sampling and superposition of the four baseband signals. We now analyze the effect of these harmonics on matching. We start by describing V_x in terms of its Fourier series

$$V_x(t) = \sum_{n=1,3,5\ldots}^{\infty} V_{x,n}(t) \quad (14)$$

with the nth harmonic, $V_{x,n}$ taking the form shown in (15) at the bottom of the page. Here we define the baseband voltages $V_I = (V_{C,0} - V_{C,2})/2$, and $V_Q = (V_{C,1} - V_{C,3})/2$. Since n is odd, the trailing $\sin(n\pi/4)$ and $\cos(n\pi/4)$ terms always have a magnitude of $1/\sqrt{2}$ but change sign with harmonic number.

The presence of odd harmonics in V_x indicates that current flowing through the antenna impedance must also contain these harmonics. Because antennas generally do not present a constant impedance across frequency, we treat impedance as being different at each harmonic of the LO, and so define a distinct antenna resistance at each harmonic: $R_a(n\omega_{LO})$. Note that for simplicity, we are assuming that $R_a(n\omega_{LO})$ is a real impedance, a description for complex antenna impedance will be provided in Section V. After once again combining the switch resistance and antenna resistance we define a new $R'_a(n\omega_{LO})$

$$R'_a(n\omega_{LO}) = R_a(n\omega_{LO}) + R_{sw}. \quad (16)$$

The current flowing through the switches can now be defined as

$$I_A(t) = \frac{V_{RF}(t)}{R'_a(\omega_{LO})} - \sum_{n=1,3,5\ldots}^{\infty} \frac{V_{x,n}(t)}{R'_a(n\omega_{LO})}. \quad (17)$$

The first term represents the current coming from the antenna through the series R'_a and the second term represents the return current due to V_x. Translating these currents back to baseband, we can once again balance charge flow into and out of each baseband capacitor for each LO cycle

$$\begin{aligned} Q_m &= \frac{V_{C,m}T_{LO}}{R_B} \\ &= \int_{mT_{LO}/4}^{(m+1)T_{LO}/4 - T_{LO}/8} I_A dt \quad m = 0,1,2,3. \end{aligned} \quad (18)$$

Substituting in (15) and (17) and solving the integral and noting that $V_{c,0} = -V_{c,2} = V_I$ and $V_{c,1} = -V_{c,3} = V_Q$, we get (19), shown at the bottom of the next page. For comparison, we apply Kirchoff's current law to the V_x node of Fig. 3, yielding a similar equation [(20), at the bottom of the next page].

$$V_{x,n}(t) = \frac{4}{n\pi}\left(V_I\cos(n\omega_{LO}t)\sin\left(\frac{n\pi}{4}\right) + V_Q\sin(n\omega_{LO}t)\cos\left(\frac{n\pi}{4}\right)\right). \quad (15)$$

Equations (19) and (20) are equivalent provided that

$$R_{sh} = \left(\sum_{n=3,5\ldots}^{\infty} \frac{1}{n^2 R'_a(n\omega_{LO})}\right)^{-1} = \left(\sum_{n=3,5\ldots}^{\infty} \frac{1}{n^2}\frac{1}{R_a(n\omega_{LO})+R_{sw}}\right)^{-1}. \quad (21)$$

Thus, we see that in the general case, R_{sh} depends upon the antenna impedance at each of the odd harmonics of the LO frequency, and represents the dissipation and/or reradiation of power due to these harmonics. If we remove the frequency dependence of R_a and perform the summation we find that this impedance is actually equal to the R_{sh} found using the charge balance method in Section II. This confirms that the virtual resistance R_{sh} which is used in the LTI model (Fig. 3) actually represents the loss due to harmonic reupconversion and dissipation.

$$\begin{aligned} R_{sh} &= \left(\sum_{n=1,3,5\ldots}^{\infty} \frac{1}{n^2}\frac{1}{R_a+R_{sw}}\right)^{-1} \\ &= \left(\left(\frac{\pi^2}{8}-1\right)\frac{1}{R_a+R_{sw}}\right)^{-1} \\ &= R'_a\frac{4\gamma}{1-4\gamma} \end{aligned} \quad (22)$$

B. Impedance as a Function of Varying IF

So far, we have made several assumptions in order generate a simple model for impedance matching. We assumed that $\omega_{IF} \rightarrow 0$, and so did not take into account the effect of the sampling capacitor C_L from Fig. 1 on the impedance seen at the antenna port. In this section we will remove the zero-IF requirement and show the effect of the baseband capacitor C_L as the input frequency varies around a constant LO.

We begin by modifying the input tone (2) to incorporate a baseband frequency ω_{IF}, such that $\omega_{RF} = \omega_{LO} + \omega_{IF}$ (where ω_{IF} can be either positive or negative), and reformulate time as $t = kT_{LO} + \tau$ so as to separate time within a given LO cycle (τ) from slow changing effects across LO cycles introduced by ω_{IF}.

$$V_{RF}(t) = A\cos((\omega_{LO}+\omega_{IF})(kT_{LO}+\tau)). \quad (23)$$

We then incorporate this new V_{RF} into the charge balance (3) (see (24) at the bottom of the page). Note that the load present at the baseband is now Z_B, which will vary in frequency as a function of ω_{IF}, and can be written as

$$Z_B(\omega_{IF}) = R_B \| (j\omega_{IF}C_L) = \frac{R_B}{1+j\omega_{IF}C_LR_B}. \quad (25)$$

After performing the integral, moving R'_a to the left side and evaluating at the limits, we compute a $V_{C,m}$ which is very similar to (4), with the arbitrary phase shift now becoming $\omega_{IF}kT_{LO}$

$$\begin{aligned} V_{C,m} = &\frac{4}{\pi}\frac{Z_B}{Z_B+4R'_a}\frac{\omega_{LO}}{\omega_{RF}}A\sin\left(\frac{\pi}{4}+\omega_{IF}\frac{T_{LO}}{8}\right) \\ &\times\cos\left(\omega_{IF}kT_{LO}+\omega_{IF}\frac{mT_{LO}}{4}+\frac{m\pi}{2}\right) \end{aligned} \quad (26)$$

which, provided that $\omega_{IF} \ll \omega_{LO}$, implies

$$\begin{aligned} V_{C,m} = &\frac{2\sqrt{2}}{\pi}\frac{Z_B}{Z_B+4R'_a}A \\ &\times\cos\left(\omega_{IF}T_{LO}\left(k+\frac{m}{4}\right)+\frac{m\pi}{2}\right). \end{aligned} \quad (27)$$

Discretized over one quarter period of the LO, the term $T_{LO}(k+m/4)$ equals t. Using this fact and extracting the up-converted

$$V_{x,1}(t)\left(\frac{1}{R_B}+\frac{2}{\pi^2R'_a(\omega_{LO})}+\sum_{n=1,3,5\ldots}^{\infty}\frac{2}{n_2\pi^2R'_a(\omega_{LO})}\right) = \frac{2}{\pi^2R'_a(\omega_{LO})}V_{RF}(t). \quad (19)$$

$$V_{x,1}(t)\left(\frac{1}{R_B}+\frac{\gamma}{Ra(\omega_{LO})}+\frac{\gamma}{R_{sh}}\right) = \frac{\gamma}{R'_a(\omega_{LO})}V_{RF}(t). \quad (20)$$

$$\begin{aligned} Q_m &= \frac{V_{C,m}T_{LO}}{Z_B} \\ &= \int_{kT_{LO}+mT_{LO}/4-T_{LO}/8}^{kT_{LO}+(m+1)T_{LO}/4-T_{LO}/8} \frac{V_{RF}-V_{C,m}}{R'_a}dt \quad m=0,1,2,3. \end{aligned} \quad (24)$$

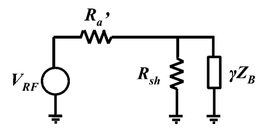

Fig. 6. New LTI equivalent circuit for frequency-dependent Z_B.

$V_x(\omega_{RF})$, we find an expression becomes essentially identical to (6)

$$V_x(\omega_{RF}) = V_{RF}(\omega_{RF})\frac{8}{\pi^2}\frac{Z_B}{Z_B + 4R_a'}. \tag{28}$$

This then produces the same derivation of the current I_A as shown above.

If we now reintroduce the LTI model with a simple transformation from γR_B to γZ_B (see Fig. 6), we can rewrite the expression for impedance seen by the antenna (11), including the frequency-dependent Z_B.

$$\begin{aligned} Z_{in}(\omega_{IF}) &= R_{sw} + \gamma Z_B(\omega_{IF}) \| R_{sh} \\ &= R_{sw} + \frac{\gamma R_B \| R_{sh}}{1 + j\omega_{IF} C_L(\gamma R_B \| R_{sh})}. \end{aligned} \tag{29}$$

Fig. 7 shows the effective real and imaginary components of the impedance seen at IF and at RF due to the frequency-dependent components. The presence of the baseband capacitor C_L has two notable effects on the tunable impedance presented to the antenna port. First, because the capacitor shunts high-frequency IF signals on the baseband port, it creates a band pass filter. As a result, the effect of tuning R_B on the impedance match diminishes for larger baseband frequencies as Z_{in} becomes dominated by C_L and ultimately approaches R_{sw} for larger offset frequencies. The presence of this band pass filter has been shown to contribute to the attenuation of out-of-band blockers resulting in measurements of $\mathrm{IIP3} > 25\ \mathrm{dBm}$ [1], [18]. Second, the imaginary component of Z_{in} looks negative for positive ω_{IF} and positive for negative ω_{IF}. This means that for a negative IF, the antenna port sees a complex conjugate of the impedance presented by the baseband. Meanwhile, the asymmetric imaginary component of Z_{in} accounts for the frequency offset of the ideal match in Fig. 5. This imaginary component is interacting with the capacitive parasitics on the RF port of the mixer, such that an ideal complex conjugate match occurs at a slight frequency offset from the LO.

IV. Noise Performance

A. Noise Performance of Passive Mixer

The time-invariant model in Fig. 3 also simplifies the calculation of the noise contributions for the mixer. To see this, we first need to look at the various sources of noise in the circuit shown in Fig. 1. There are three fundamental sources of noise: the baseband resistance R_B, the switch resistance, R_{sw}, and the thermal noise from the antenna itself, R_a. As before, we can safely merge the antenna and switch resistance into a single resistor, R_a'. To find the total noise, we compute the total noise current injected into the baseband node, and multiply this with the total impedance at that node. Thus, if R_B is a real resistor, this current will be: $i_{n,b}^{*2} = 4kT/\gamma R_B$.

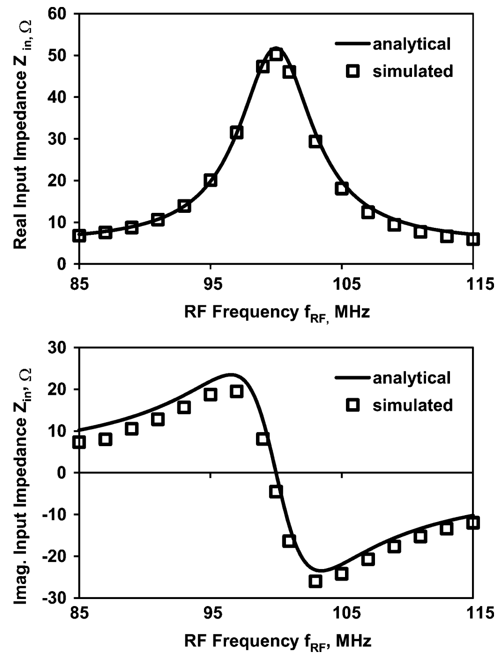

Fig. 7. Effective real and imaginary components of Z_{in} as a function of RF frequency.

Similarly the noise from R_a' is $i_{n,a'}^{*2} = 4kT/R_a'$. However, to be complete, this noise must also include noise down-converted by the mixer at odd harmonics of the LO, such that $i_{n,a'}^{*2}(n\omega_{LO}) = 4kT/n^2 R_a'(n\omega_{LO})$. The schematic on the left side of Fig. 8 shows this model. However, we note that the sum of the antenna noise currents $i_{n,a'}^{*2}(n\omega_{LO})$ for $n = 3, 5, 7$, etc., is exactly the noise that would be generated by R_{sh} if it was a real resistor. Therefore we can use the two noise models in Fig. 8 interchangeably. The total noise voltage is the sum of the thermal voltage sources corresponding to each resistor in the circuit. The noise factor for this circuit is found by dividing the total output noise by the portion of that noise caused by the input noise of R_a

$$\begin{aligned} F = 1 + \frac{v_{n,sw}^{*2}}{v_{n,a}^{*2}} + \frac{v_{n,sh}^{*2}}{v_{n,a}^{*2}}\left(\frac{R_a + R_{sw}}{R_{sh}}\right)^2 \\ + \frac{v_{n,B}^{*2}}{v_{n,a}^{*2}}\left(\frac{R_a + R_{sw}}{\gamma Z_B}\right)^2. \end{aligned} \tag{30}$$

If we assume impedance matching to 50 Ω and a switch resistance of 5 Ω, this results in $NF = 3.88\ \mathrm{dB}$. Note that this noise is dominated by contributions from the baseband resistor R_B and includes no noise from subsequent amplifiers. In the next section we will demonstrate how this noise contribution can be minimized in the implementation of an actual receiver using the passive mixer-first architecture.

B. Receiver Architecture

In order to add gain to the receiver and to improve its noise figure, all while maintaining the impedance matching functionality through the passive mixer, we have proposed the receiver architecture shown in Fig. 10 [1]. This receiver consists of a passive quadrature mixer, followed by baseband amplifiers in re-

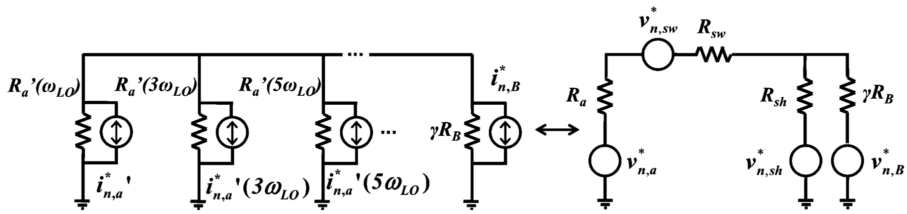

Fig. 8. Equivalent noise models for LTI model from Fig. 3.

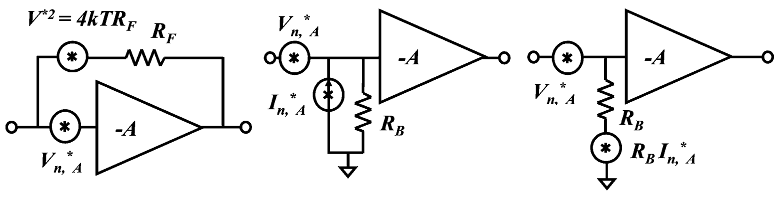

(a) (b) (c)

Fig. 9. Equivalent baseband amplifier noise models.

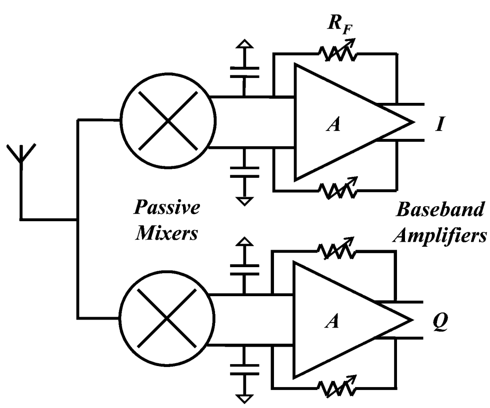

Fig. 10. Proposed passive-mixer first receiver with resistive feedback amplifiers.

sistive feedback. We find the new effective R_B present on each branch by applying the Miller effect to the feedback resistor R_F:

$$R_B = \frac{R_F}{1+A}. \tag{31}$$

Substituting the new R_B into the impedance matching LTI model shows that we can perform impedance matching using the amplifier feedback resistors.

Once we have added the feedback amplifiers to implement R_B, the noise performance changes as well. Whereas most of the noise sources in (30) can be treated as standard resistive thermal noise, the baseband noise is now due to the feedback resistor and the input referred noise of the amplifier itself [Fig. 9(a)]. This noise is traditionally modeled by a pair of correlated noise sources: a series voltage and shunt current [Fig. 9(b)]. This is equivalent to two voltage sources, as shown on the right of Fig. 9(c).

These two sources both depend upon the input referred voltage noise of the amplifier, and so are correlated. However, the source present in shunt also depends upon the feedback resistor and amplifier gain, and can be computed to be

$$i_{n,A}^{*2} R_B^2 = \left(\frac{4kTR_F}{(A+1)^2} + \frac{v_{n,A}^{*2}}{(A+1)^2} \right). \tag{32}$$

Substituting the equation for thermal noise and (32) into (30), and accounting for γ both in the baseband noise (by multiplying

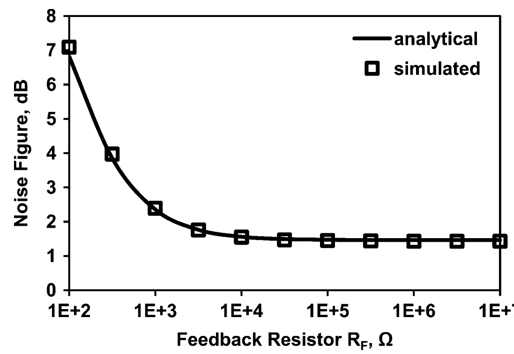

Fig. 11. Simulated and analytical noise figure versus feedback resistor R_F.

the squared noise by γ) and in the baseband resistance (by multiplying R_B by γ), yields the following noise factor:

$$\begin{aligned} F = 1 &+ \frac{R_{sw}}{R_a} + \frac{R_{sh}}{R_a}\left(\frac{R_a+R_{sw}}{R_{sh}}\right)^2 \\ &+ \gamma\frac{R_F}{R_a}\left(\frac{R_a+R_{sw}}{\gamma R_F}\right)^2 + \gamma\frac{v_{n,A}^{*2}}{4kTR_a} \\ &\times \left(\frac{R_a+R_{sw}}{\gamma R_F} + \frac{R_a+R_{sw}+R_{sh}}{R_{sh}}\right)^2. \end{aligned} \tag{33}$$

We have verified this relationship (see Fig. 11) with simulation using periodic steady state analysis in SpectreRF, with $f_{LO} = 100\,\mathrm{MHz}$, $A = 30$, $v_{n,A}^* = 400\,\mathrm{pV}/\sqrt{\mathrm{Hz}}$, and the same device parameters as in Fig. 4. The simulation results match analyitical predictions well.

By making baseband gain A (and so R_F) large, and biasing the amplifier with sufficient current to make $v_{n,A}^{*2}$ small, the latter terms can be made small. Furthermore, by choosing transistor dimensions such that the switch resistance and therefore its noise are small relative to R_a, we find a limit on the noise factor which depends on R_{sh}

$$F > 1 + \frac{R_a}{R_{sh}}. \tag{34}$$

For constant $R_a'(\omega)$, where (10) holds, (34) implies that $F > 1.23$, or $NF = 0.91$ dB. In cases where antenna impedance decreases with frequency, this limit is degraded. More generally, Provided that $R_{sh} \gg R_a$, $R_{sw} \ll R_a$, and $R_F \gg R_a$, all of these terms will be much less than one except the final term which also depends upon amplifier noise. Under these conditions, the baseband amplifier can be expected to limit noise figure. Indeed, amplifier noise has been reported as the dominant noise source in existing work [1], [9], [10].

It is worth noting, however, that the effect of baseband amplifier noise is also dependent on the value of R_{sh}, and will degrade strongly as R_{sh} is made small. The effect of R_{sh} on both the impedance matching range and NF of passive mixers shows that neglecting the effects of reupconversion of baseband signals to higher harmonics will result in an inaccurate model.

V. Complex Antenna Impedance

A. Effects of Complex Antenna Impedance

Thus far, the model we have presented assumes a purely real antenna impedance. We will now expand this treatment to incorporate a complex antenna impedance $Z_a(\omega)$. Such a complex impedance can appear either directly on the antenna as it is used across wide frequency ranges, and also through bond wires, pads, and parasitic capacitances on the switches themselves.

By performing the analysis is Section II again, except with the inclusion of $Z'_a = Z_a(\omega_{LO}) + R_{sw}$, we find a new model which is very similar to the previous one except with the replacement of R_a with Z_a. This means that the harmonic shunting impedance will also be complex, so we rename it Z_{sh}. Z_{sh} can be computed as above in (18)–(21), but including phase shifts in the current due to the harmonics of V_x. Because the effects of these phase shifts depend upon which harmonic is being shifted, this calculation results in a Z_{sh} that incorporates Z_a for the 5th, 9th, 13th, etc., harmonic of ω_{LO} and the complex conjugate of Z_a (Z_a^*) for the 3rd, 7th, 11th, etc. See (35) at the bottom of the page. Using these, we can rewrite the expression for Z_{in} similar to that derived from Fig. 3.

$$Z_{in} = R_{sw} + \gamma Z_B \| Z_{sh}. \tag{36}$$

We confirmed the analysis leading to (29) with numerical simulations, using the same model as in Fig. 4, and sweeping LO frequency, but with 300 fF of parasitic capacitance on the RF port of the mixer (in parallel with 150 fF parasitic capacitance from the switch transistors themselves) and setting $R_F = 2660\ \Omega$. As can be seen in Fig. 12, this demonstrates close agreement between analysis and simulation. Additionally, we may write an expression for noise factor similar to (33)

$$\begin{aligned} F = 1 &+ \frac{R_{sw}}{\mathrm{Re}(R_a)} + \frac{\mathrm{Re}(Z_{sh})}{\mathrm{Re}(Z_a)} \left| \frac{Z_a + R_{sw}}{Z_{sh}} \right|^2 \\ &+ \frac{\gamma R_F}{\mathrm{Re}(Z_a)} \left| \frac{Z_a + R_{sw}}{\gamma R_F} \right|^2 + \frac{\gamma v_{n,A}^{*2}}{4kT\mathrm{Re}(Z_a)} \\ &\times \left| \frac{Z_a + R_{sw}}{\gamma R_F} + \frac{Z_a + R_{sw} + R_{sh}}{R_{sh}} \right|^2. \end{aligned} \tag{37}$$

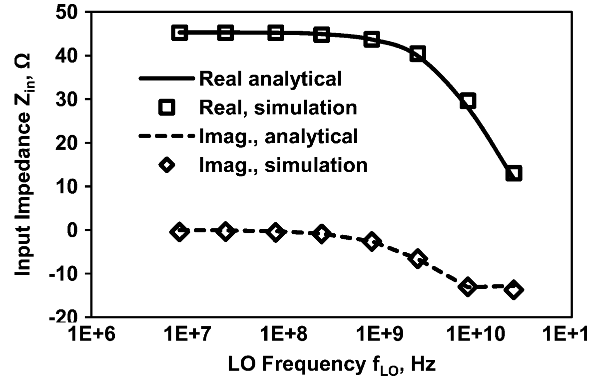

(a)

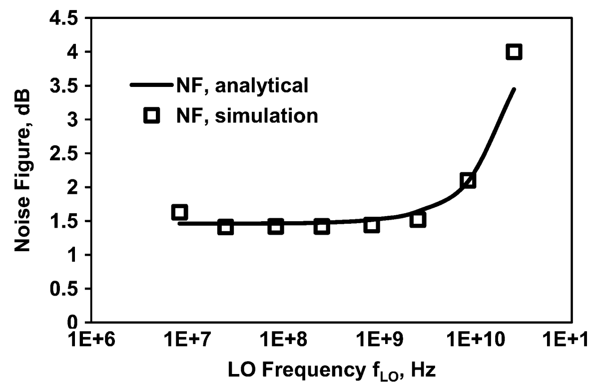

(b)

Fig. 12. Comparison of analytical and simulated receiver a) input impedance, and b) noise figure versus frequency, accounting for frequency-dependent antenna impedance.

B. Matching to a Complex Antenna Impedance: Complex Feedback

In this formulation, the antenna impedance and shunt impedance can both take on complex values, and a complex conjugate match will only be achieved if the complex component of Z_B is tunable. With the architecture described so far, making the capacitor C_L tunable would provide this, but only as a negative reactance, and would also strongly affect the bandwidth of the match. Instead, in order to introduce the complex term in the context of the circuit shown in Fig. 10, we can modify the original baseband amplifiers by applying additional feedback resistors from the I to the Q channel and the Q to the I channel as shown in Fig. 13. A similar feedback technique is utilized in [19] but was used to modify the phase of a filter rather than to present a complex impedance to the input.

In order to analyze this circuit, we will begin with a simple case where we define the signal coming from the antenna as

$$V_{RF}(t) = \cos(\omega_{LO} t). \tag{38}$$

$$Z_{sh}(n\omega_{LO}) = \left(\sum_{n=3,7,11\ldots}^{\infty} \frac{1}{n^2 Z_a'^{*}(n\omega_{LO})} + \sum_{n=5,9,13\ldots}^{\infty} \frac{1}{n^2 Z'_a(n\omega_{LO})} \right)^{-1}. \tag{35}$$

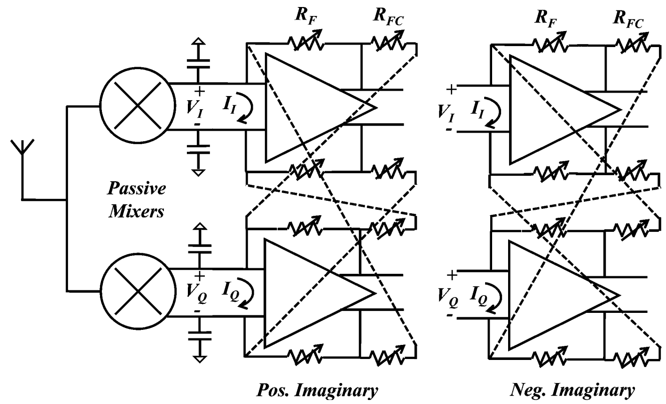

Fig. 13. Positive and negative complex feedback applied to the baseband amplifier.

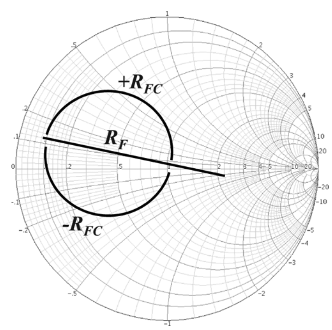

Fig. 14. Simulated S_{11} Smith chart for varying $\pm R_{FC}$.

When this signal is down-converted through the I and Q paths of the mixer, assuming the two paths are perfectly balanced, we should get

$$\begin{aligned} V_I &= 1 \\ V_Q &= 0. \end{aligned} \tag{39}$$

We then look at the amplitude of the current present at the inputs of the amplifiers due to the new cross-connected feedback resistors we see

$$\begin{aligned} I_I &= \frac{V_I(1+A)}{R_F} + \frac{V_I}{R_{FC}} \\ I_Q &= \frac{V_I A}{R_{FC}}. \end{aligned} \tag{40}$$

Equation (40) shows that the cross-channel feedback connections introduce a scaled 90° out of phase component of V_{RF} back to the input. When these currents are back upconverted to the antenna port, we find

$$\begin{aligned} I_{RF} &= I_I \cos(\omega_{LO} t) + I_Q \sin(\omega_{LO} t) \\ &= \left(\frac{V_I(1+A)}{R_F} + \frac{V_I}{R_{FC}} \right) \cos(\omega_{LO} t) \\ &\quad + \frac{V_I A}{R_{FC}} \sin(\omega_{LO} t). \end{aligned} \tag{41}$$

Using (41) we may write an expression for the effective complex baseband impedance, Z_B, where the sign of the imaginary term depends on whether the feedback is connected in positive or negative complex feedback (see Fig. 13)

$$Z_B = \left[\left(\frac{1+A}{R_F} + \frac{1}{R_{FC}} \right) \pm j \frac{A}{R_{FC}} \right]^{-1}. \tag{42}$$

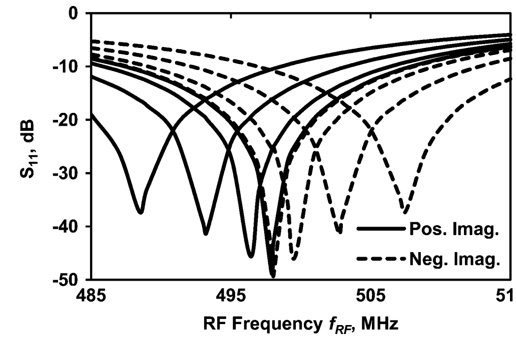

Fig. 15. Simulated S_{11} for varying $\pm R_{FC}$ showing shift in center frequency of optimal match.

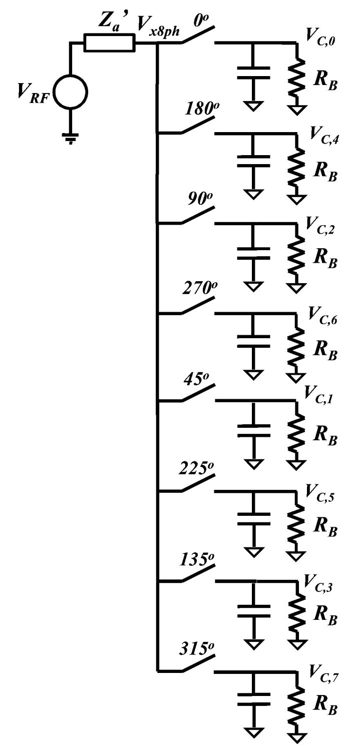

Fig. 16. Eight-phase passive mixer.

Note that if we repeat this analysis for the case where $V_{RF} = \sin(\omega_{LO} t)$, we find that because of the relative phases of sin and cos, we actually need to flip the polarity of the feedback resistors from the Q channel to the I channel, in order to get the same equivalent complex phase shift. This result is seen in the schematic in Fig. 13.

Using a similar simulation setup to Fig. 5, Fig. 14 shows an S_{11} Smith-chart of the sweeps of both the real feedback resistor R_F and the complex feedback resistor R_{FC}. This figure demonstrates the distinct complex nature of the impedance presented to the antenna port using complex feedback. The sweep using R_F alone shows some complex impedance due to the parasitic capacitances present on the switches.

Fig. 15 shows an S_{11} plot of sweeps of frequency for varying complex feedback resistor R_{FC}. Here we have chosen the value of R_F from Fig. 5 which provided the best match to $R_a = 50\,\Omega$. However as we noted earlier, this match was narrowband and centered around 497 MHz. Fig. 15 shows that complex feedback can change this center frequency to either side of the LO by interacting with the imaginary component of the antenna impedance and of the baseband capacitors. Each curve is for a different value of R_{FC}, with smaller resistors pushing the center frequency further from the LO.

VI. Limitations of 4-Phase Mixing and Benefits of More LO Phases

A. Implications of Z_{sh}

One implication of (11), (29), and (36) is that in order to maximize impedance tuning range and minimize noise figure, it is desirable to maximize Z_{sh}. Equation (35) in turn shows that maximizing Z_{sh} requires maximizing the impedance presented to the RF port of the mixer at higher harmonics of the LO frequency. Note that this is exactly the opposite result from that typically created by simple resonant matching networks, where shunting parasitic capacitance reduces impedance at higher frequencies, and a resonant network maximizes impedance at the fundamental [9].

Another implication is that noise figure is not necessarily minimized by simply reducing switch resistance. Since parasitic capacitance on the mixer input acts to shunt Z_a, driving $Z_a(\omega) \to 0$, and therefore $Z'_a(\omega) \to R_{sw}$ as $\omega \to \infty$. Under this condition, reduction in R_{sw} will also act to reduce Z_{sh}. Furthermore, widening the mixer transistors to reduce R_{sw} will also increase the parasitic capacitance on the mixer input, further reducing Z_{sh}. Thus, it is expected that intermediate width mixer devices with small but finite switch resistance will provide optimal noise, especially under resonant match. This can be analyzed for the extreme case of a very high-Q antenna with impedance R_a near ω_{LO}, but zero at harmonics of ω_{LO}. In this case, $R_{sh} = 4.3R_{sw}$, and so

$$NF = 1 + \frac{R_{sw}}{R_a} + \frac{(R_a + R_{sw})^2(1-4\gamma)}{4\gamma R_a R_{sw}} \tag{43}$$

(neglecting baseband noise entirely). The NF is minimum when

$$R_{sw} = R_a\sqrt{1-4\gamma} \Rightarrow NF \geq 4.05\ \text{dB}. \tag{44}$$

No matter how high an impedance is achieved by a high-Q resonant match, NF will always be worse than 3 dB, whereas a wider band match can actually provide lower NF.

B. Enhancements Due to Multiphase Mixers

It is clear that performance improves as Z_{sh} is increased, and as (35) shows, Z_{sh} can be considered to be a parallel combination of the antenna and switch impedance computed at each of the odd harmonics of the LO, weighted by the harmonic number. This harmonic impedance dependence is a consequence of the harmonic content of the virtual voltage $V_x(t)$. For the switching waveforms in Fig. 2, $V_x(t)$ contains all of the odd harmonics of ω_{LO}, weighted by one over the harmonic number, and so dissipates or reradiates power at all of these frequencies. This indicates that if an alternate mixer structure was chosen which provided for a less harmonic rich V_x, reradiation would be reduced, and consequently Z_{sh} made larger. One such structure is the 8-phase passive mixer shown in Fig. 16, driven by eight nonoverlapping LO signals similar in concept to "harmonic suppression mixers" recently discussed in the literature [1], [13], [18], [20].

Using such a mixer and the definition of V_{RF} from (2), we can compute that the four differential outputs will take the form

$$\begin{aligned}
V_{C,0} - V_{C,4} &= GA(t)\cos(\phi(t)+\theta)\\
V_{C,1} - V_{C,5} &= GA(t)\cos\left(\phi(t)+\theta-\frac{\pi}{4}\right)\\
&= \frac{GA(t)}{\sqrt{2}}(\sin(\phi(t)+\theta)+\cos(\phi(t)+\theta)\\
V_{C,2} - V_{C,6} &= GA(t)\cos\left(\phi(t)+\theta-\frac{\pi}{2}\right)\\
&= GA(t)(\sin(\phi(t)+\theta)\\
V_{C,3} - V_{C,7} &= GA(t)\cos\left(\phi(t)+\theta-\frac{3\pi}{4}\right)\\
&= \frac{GA(t)}{\sqrt{2}}(\sin(\phi(t)+\theta)-\cos(\phi(t)+\theta)
\end{aligned} \tag{45}$$

where the constants G and θ are introduced to account for the effects of Z'_a and Z_B. The key point here is that the down sampling of this mixer results in outputs with exactly the relative weights needed for harmonic suppression when back up-converted, without any explicit weighting circuitry. Thus V_{x8ph}, which takes the form shown in Fig. 17, has a Fourier series which only contains half of all odd harmonics, driving the terms corresponding to $n = 3,\ 5,\ 11,\ 13, \ldots$ to zero.

This reflects in Z_{sh}, which, following a derivation similar to (35), is as shown in (46) at the bottom of the page.

Once again, half of the odd harmonics are eliminated, dramatically increasing Z_{sh}. The complex version of the model in Fig. 3 still applies, using this new Z_{sh} and altering the term γ, such that

$$\gamma_{8ph} = \frac{2}{\pi^2}(2-\sqrt{2}) \approx 0.119. \tag{47}$$

Substituting (46) and (47) into (36) and (37) allows us to compute input impedance and noise figure. In the case of constant, real antenna resistance, analogous to (10), the 8-phase mixer provides a shunting resistance of

$$R_{sh8ph} = R'_a \frac{8\gamma_{8ph}}{1-8\gamma_{8ph}} \approx 18.9R'_a. \tag{48}$$

$$Z_{sh}(n\omega_{LO}) = \left(\sum_{n=7,15\ldots}^{\infty} \frac{1}{n^2 Z'^*_a(n\omega_{LO})} + \sum_{n=9,17\ldots}^{\infty} \frac{1}{n^2 Z'_a(n\omega_{LO})}\right)^{-1}. \tag{46}$$

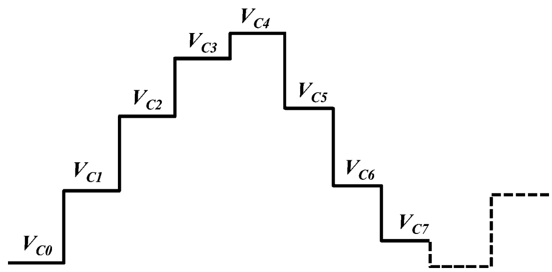

Fig. 17. Approximation of waveform V_{x8ph} for 8-phase mixer.

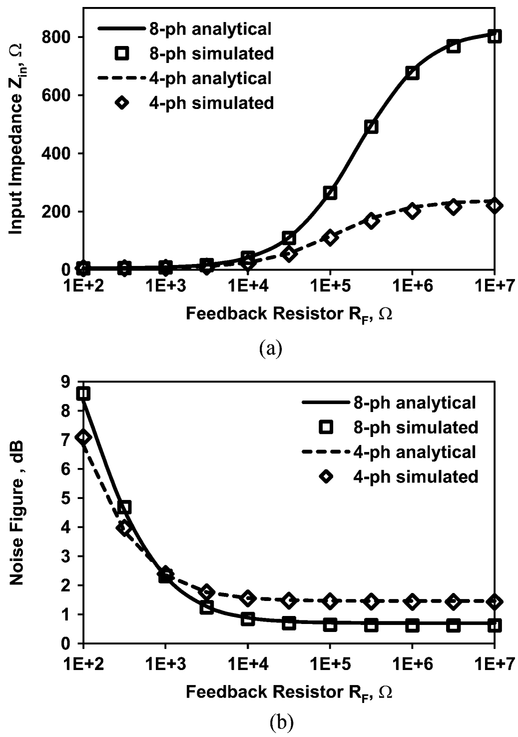

Fig. 18. Comparison of (a) input impedance and (b) noise figure between 4-phase and 8-phase mixers.

This is almost five times larger than the 4-phase case. Furthermore, applying the fundamental limit to NF from (34) to the 8-phase case, we find that NF > 0.22 dB for a constant antenna impedance. These results are confirmed by numerical simulation in Fig. 18, and show both a much larger input impedance range and lower noise figure for an 8-phase mixer than for a 4-phase mixer. Note that the analytical result for the input impedance in Fig. 18 must take into account the parasitic shunt capacitance on the antenna port, even at 100 MHz. This is because higher harmonics of the LO now dominate Z_{sh}, and since the capacitor has more effect at these higher frequencies, its contribution to Z_{sh} is greater. For the case of a high-Q match as in (43) and (44), NF is best when

$$R_{sw} = R_a \sqrt{1 - \frac{16(2-\sqrt{2})}{\pi^2}} \Rightarrow NF \geq 2\,\mathrm{dB} \qquad (49)$$

which implies that even for a high Q match, good NF is possible with eight nonoverlapping LO phases.

VII. Conclusion

The analyses and simulations presented here reveal several important facts about passive mixer-first receivers. The first is that for quadrature passive mixers using nonoverlapping clocks, the input impedance at the RF port of the device is strongly sensitive to the impedance presented to the baseband ports of the mixer, and increasing the baseband resistance acts to increase the apparent RF resistance, allowing for baseband-controlled impedance matching. Second, this method can be expanded with baseband feedback between in-phase and quadrature paths to implement a complex conjugate impedance match at the RF port. A third important point is that the degree to which the baseband impedance can influence the RF impedance depends on reradiation back through the mixer at higher harmonic frequencies. In particular, this results in a shunting effect which in turn depends on the impedance presented to the mixer's RF port at these higher harmonics: lower impedance at harmonic frequencies translates to more shunting. Meanwhile, suppression of these harmonics with appropriate mixer design can reduce this shunting effect significantly, improving performance. What holds for impedance also holds for noise, with noise figure depending on both the antenna and baseband impedance, and with increased harmonic shunting degrading this NF. Finally, we have shown that with appropriate baseband design, the fundamental limit on noise figure in a passive mixer-first receiver is set by this shunting or reradiation effect, and can be lower than 3 dB.

References

[1] C. Andrews and A. C. Molnar, "A passive-mixer-hirst receiver with baseband-controlled RF impedance matching > 6 dB NF, and < 27 dBm wideband IIP3," in *ISSCC Dig. Tech. Papers*, Feb. 2010, vol. 53, pp. 46–47.

[2] J. Liu, G. Vandersteen, J. Craninckx, M. Libois, M. Wouters, F. Petre, and A. Barel, "A novel and low-cost analog front-end mismatch calibration scheme for MIMO-OFDM WLANS," in *Proc. IEEE Radio Wireless Symp.*, Jan. 2006, pp. 219–222.

[3] A. van Bezooijen, M. de Jongh, C. Chanlo, L. Ruijs, F. van Straten, R. Mahmoudi, and A. van Roermund, "A GSM/EDGE/WCDMA adaptive series-LC matching network using RF-MEMS switches," *IEEE J. Solid-State Circuits*, vol. 43, no. 10, pp. 2259–2268, Oct. 2008.

[4] J. Craninckx, M. Liu, D. Hauspie, V. Giannini, T. Kim, J. Lee, M. Libois, D. Debaillie, C. Soens, M. Ingels, A. Baschirotto, J. V. Driessche, L. V. der Perre, and P. Vanbekbergen, "Fully reconfigurable software-defined radio transceiver in $0.13\ \mu$m CMOS," in *ISSCC Dig. Tech. Papers*, Feb. 2007, pp. 346–347.

[5] A. Bourdoux, J. Craninckx, A. Dejonghe, and L. V. der Perre, "Receiver architectures for software-defined radios in mobile terminals: The path to cognitive radios," in *Proc. IEEE Radio Wireless Symp.*, Jan. 2007, pp. 535–538.

[6] R. v. d. Beek, J. Bergerboet, H. Kundur, D. Leenaerts, and G. Weide, "A 0.6-to-10 GHz receiver front-end in 45 nm CMOS," in *ISSCC Dig. Tech. Papers*, Feb. 2008, pp. 128–129.

[7] J.-H. Zhan and S. Taylor, "A 5 GHz resistive-feedback CMOS LNA for low-cost multi-standard,applications," in *ISSCC Dig. Tech. Papers*, Feb. 2006, pp. 721–730.

[8] W.-H. Chen, G. Liu, B. Zdravko, and A. Niknejad, "A highly linear broadband CMOS LNA employing noise and distortion cancellation," *IEEE J. Solid-State Circuits*, vol. 43, no. 5, pp. 1164–1176, May 2008.

[9] B. Cook, A. Berny, A. Molnar, S. Lanzisera, and K. Pister, "Low power 2.4 GHz transceiver with passive RX front-end and 400 mV supply," *IEEE J. Solid-State Circuits*, vol. 41, no. 12, pp. 2757–2766, Dec. 2006.

[10] M. Soer, E. Klumperink, Z. Ru, F. V. van, and B. Nauta, "A 0.2-to-2.0 GHz 65 nm CMOS receiver without LNA achieving 11 dBm IIP3 and 6.5 dB NF," in *ISSCC Dig. Tech. Papers*, Feb. 2009, pp. 222–223.

[11] S. Zhou and M.-C. Chang, "A CMOS passive mixer with low flicker noise for low-power direct-conversion receiver," *IEEE J. Solid-State Circuits*, vol. 40, no. 5, pp. 1084–1093, May 2005.

[12] A. Mirzaei, H. Darabi, J. Leete, X. Chen, K. Juan, and A. Yazdi, "Analysis and optimization of current-driven passive mixers in narrowband direct-conversion receivers," *IEEE J. Solid-State Circuits*, vol. 44, no. 10, pp. 2678–2688, Oct. 2009.

[13] A. Molnar, B. Lu, S. Lanzisera, B. Cook, and K. Pister, "An ultralow power 900 MHz RF transceiver for wireless sensor networks," in *Proc. IEEE Custom Integr. Circuits Conf.*, Oct. 2004, pp. 401–404.

[14] N. Kim, L. Larson, and V. Aparin, "A highly linear saw-less CMOS receiver using a mixer with embedded Tx filtering for CDMA," *IEEE J. Solid-State Circuits*, vol. 44, no. 8, pp. 2126–2137, Aug. 2009.

[15] D. Kaczman, M. Shah, M. Alam, M. Rachedine, D. Cashen, L. Han, and A. Raghavan, "A single chip 10-band WCDMA/HSDPA 4-band GSM/EDGE SAW-less CMOS receiver with DigRF 3G interface and $+90\ \mathrm{dBm}$ IIP2," *IEEE J. Solid-State Circuits*, vol. 44, no. 3, pp. 718–739, Mar. 2009.

[16] H. Khatri, L. Liu, T. Chang, P. Gudem, and L. Larson, "A SAW-less CDMA receiver front-end with single-ended LNA and single-balanced mixer with 25% duty-cycle LO in 65 nm CMOS," in *Proc. IEEE Radio Freq. Integr. Circuits Symp.*, Jun. 2009, pp. 13–16.

[17] M. Camus, B. Butaye, L. Garcia, M. Sie, B. Pellat, and T. Parra, "A $5.4\ \mathrm{mW}/0.07\ \mathrm{mm}^2$ 2.4 GHz front-end receiver in 90 nm CMOS for IEEE 802.15.4 WPAN standard," *IEEE J. Solid-State Circuits*, vol. 43, no. 6, pp. 1372–1383, Jun. 2008.

[18] Z. Ru, E. Klumperink, G. Wienk, and B. Nauta, "A software-defined radio receiver architecture robust to out-of-band interference," in *ISSCC Dig. Tech. Papers*, Feb. 2009, pp. 230–231.

[19] K.-W. Cheng, K. Natarajan, and D. Allstot, "A current reuse quadrature GPS receiver in $0.13\ \mu\mathrm{m}$ CMOS," *IEEE J. Solid-State Circuits*, vol. 45, no. 3, pp. 510–523, Mar. 2010.

[20] J. Weldon, R. Narayanaswami, J. Rudell, L. Lin, M. Otsuka, S. Dedieu, L. Tee, K.-C. Tsai, C.-W. Lee, and P. Gray, "A 1.75-GHz highly integrated narrow-band CMOS transmitter with harmonic-rejection mixers," *IEEE J. Solid-State Circuits*, vol. 36, no. 12, pp. 2003–2015, Dec. 2001.

Caroline Andrews (S'09) received the B.S. degree in electrical engineering from the University of Virginia, Charlottesville, in 2008. She is currently working toward the Ph.D. degree in electrical engineering at Cornell University, Ithaca, NY.

Her research focuses on developing highly tunable front-ends for software-defined radios.

Alyosha C. Molnar (S'05–M'07) received the B.S. degree in engineering with highest honors from Swarthmore College, Swarthmore, PA, in 1997, and the M.S. and Ph.D. degrees in electrical engineering from the University of California, Berkeley, in 2003 and 2007, respectively.

From 1998 to 2002, he was with the RF IC Group at Conexant Systems, Inc. (now Skyworks Solutions, Inc.), Newport Beach, CA, where he developed their first-generation GSM direct conversion receiver. In August 2007, he joined the faculty of the School of Electrical and Computer Engineering, Cornell University, Ithaca, NY.